ADVANCED ENGINEERING MATERIALS
www.aem-journal.com

Behavior of Different β Stabilizers on the Microstructure and Properties of Ternary Ti-3Sn-X Alloys

Leandro Bolzoni, Stella Raynova, Fei Yang, and Karl Dahm*

The manufacturing of Ti alloys via powder metallurgy and the development of novel compositions are two strategies to reduce the cost of Ti, which is still the primary factor deterring its wider use in engineering applications. In this study, new Ti alloys based on the combined addition of Sn with Nb, Mo, or Mn are manufactured via powder metallurgy to gain an understanding of the role of these β stabilizers on the performance achievable. It is found that the designed alloys have a fully homogeneous chemistry regardless of their actual composition and a lamellar or β-type microstructure depending on the actual β stabilizer used. This study confirms that the β-stabilizing power effect decreases from Mn to Mo and, eventually, Nb. The compressibility and sinterability of the alloys increase with the progressive addition of the selected powders, generally leading to stronger and more ductile materials. It is also found that the proposed Ti-3Sn-Mo alloys are characterized by the best strength/ductility pairs compared to a variety of sintered or cast binary/ternary Ti alloys bearing the alloying elements considered in this work.

1. Introduction

Titanium (Ti) and its alloys are characterized by two fundamental aspects that define their applicability in engineering products, namely, the combination of properties they provide and their high cost compared to other structural alloys.[1–3] In terms of properties, Ti alloys show the overall best combinations including low density, high strength, good corrosion resistance, and biocompatibility; however, Ti is difficult to extract and process due to its high affinity for oxygen, making it expensive.[4–6] Powder metallurgy is the ideal manufacturing technique for aiming to reduce the processing costs of Ti alloys as they are near-net-shape, solid-state methods with high yield of material utilization.[7–9]

Apart from using powder metallurgy, another strategy to reduce the cost of Ti alloys is considering cheaper alloying elements than the ones conventionally used. Such an approach is also key for the development of novel compositions with enhanced mechanical performance.[10–12] Because Ti is characterized by allotropism, alloying elements are divided between α and β stabilizers depending on whether they, respectively, raise or lower the allotropic phase transformation temperature. β stabilizers are further subdivided between isomorphous and eutectoids as a function of their overall solubility in Ti. Al is the most commonly used α stabilizer but Sn, which is a much weaker α stabilizer generally classified as neutral element, has also been considered due to its large solubility, enhancement of densification during sintering, and strengthening effect. For example, Liu et al.[13] studied the densification behavior and mechanical properties of binary Ti-(2.5–7.5)Sn alloys obtained by press (uniaxial, 300 MPa) and sinter (1100–1400 °C/2 h) of elemental powders. Compositions are in percentage by mass unless otherwise specified. Azmat et al.[14] also studied the conventional powder metallurgy route but considered a wider range of binary Ti-(5–20)Sn alloys and used cold isostatic pressing rather than uniaxial pressing for shaping the blended elemental powder blends. Finally, Ye et al.[15] produced binary Ti-(5–25)Sn alloys via spark plasma sintering at 1150 °C for 1 h under an applied pressure of 30 MPa and vacuum atmosphere analyzing the dynamic recrystallization, grain refinement, and strengthening mechanism induced by hot extrusion.

Regarding β stabilizers, Nb is generally used because it is nontoxic and permits to reduce the intrinsic stiffness, Mo is added because of its high solubility and strengthening effect while Mn is considered to reduce the cost and remarkably increase the mechanical properties. It is worth mentioning that both Nb and Mo are isomorphous whereas Mn is a eutectoid β stabilizer. Studies on the manufacturing and properties of binary Ti-Nb, Ti-Mo, and Ti-Mn alloys are available in the literature. Examples of such studies, especially when the alloys were manufactured via powder metallurgy, are the work of Zhao et al.[16] Sochacka et al.[17] and Fernandes Santos et al.[18] respectively. Specifically, Zhao et al.[16] manufactured β-type Ti-(10-22)Nb alloys by metal injection molding using elemental Ti and Nb powders sintered at 1500 °C for 2 h. Sochacka et al.[17] studied

L. Bolzoni, S. Raynova, F. Yang
School of Engineering
The University of Waikato
Hamilton 3240, New Zealand
E-mail: bolzoni.leandro@waikato.ac.nz

K. Dahm
Callaghan Innovation
Lower Hutt 5040, New Zealand

The ORCID identification number(s) for the author(s) of this article can be found under https://doi.org/10.1002/adem.202301503.

DOI: 10.1002/adem.202301503

β-type Ti-(18–52)Mo alloys shaped by both cold (600 MPa) and hot compaction and sintered in the 600–1000 °C temperature range during 1 h. Fernandes Santos et al.[18] developed β-type Ti-(8–17)Mn alloys using metal injection molding for shaping and vacuum sintering at 1100 °C for 8 h for densification.

Studies in which the combined addition of Sn and one of the previously mentioned β stabilizers to create ternary Ti alloys was analyzed are much less available in the literature, especially when using powder metallurgy. For instance, Yılmaz et al.[19] prepared ternary Ti-(0–4)Sn-16Nb alloys using metal injection molding followed by sintering (1250–1550 °C/2 h) to quantify the hardness and modulus of elasticity, but no tensile behavior was reported. Maeshima and Nishida[20] considered ternary Ti-(1–5)Sn-(5–6)Mo alloys prepared by arc melting in an Ar atmosphere to measure their shape memory properties in convenient bending and heating tests. Zhou et al.[21] recently reported the mechanical properties and corrosion behavior of ternary Ti-2Sn-(2–4)Mn alloys uniaxially pressed (600 MPa) and isothermally sintered (1100–1250 °C/1–2 h).

From the literature, it is clear that binary Ti alloys individually bearing Sn, Nb, Mo, or Mn were widely studied but ternary alloys where Sn was combined with Nb, Mo, or Mn are not properly developed, especially if manufactured via powder metallurgy. Furthermore, the understanding around their tensile behavior and its relationship with corresponding microstructures is lacking. Therefore, the aim of this work is to gain a better understanding of the role that Nb, Mo, or Mn as β stabilizers have on the microstructure and tensile properties of ternary Ti-3Sn-X alloys. Consequently, Ti-3Sn-X alloys (x = Nb, Mo, Mn) compositions were designed on the basis of currently available theories, manufactured via the classical press and sinter powder metallurgy route, and characterized in terms of microstructural, physical, and mechanical properties. It is worth remarking that press and sinter was chosen as the manufacturing process because it is a recognized high-energy efficient green technology with intrinsic advantages for processing Ti alloys. This includes being near-net-shape, which reduces the amount of machining/finishing operations needed, being solid-state, which is beneficial to limit the reactivity of Ti with manufacturing tools and atmospheric gases, and having high material's yield, which minimizes the amount of costly scrap generated during manufacturing. On top of that, the blended elemental approach used allows maximum flexibility in designing new Ti alloy compositions.

2. Experimental Section

This study considered Ti-3Sn-X alloys (x = Nb, Mo, Mn) produced via powder metallurgy. Commercially available powders were used as raw materials and their morphology and characteristics are shown in **Figure 1** and **Table 1**, respectively. The Ti powder has maximum particle size of 75 μm and irregular morphology, which is ideal for its processing via press and sinter. The powders of the alloying elements all have a variety of particle shapes and smaller particle size aiming at improving the sinterability of the alloys. It is worth mentioning that the starting Ti powder has an oxygen content of 0.23 wt%.

Ti-3Sn-X alloys powder blends were prepared via mixing through a V-blender operated at 45 Hz for 30 min. After mixing,

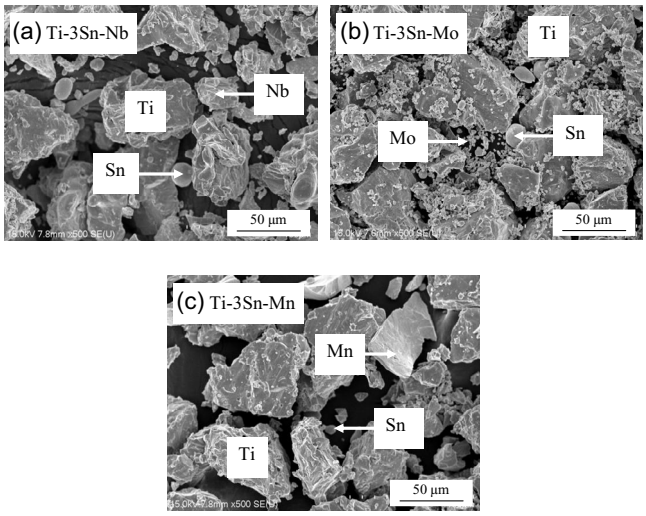

Figure 1. Representative scanning electron microscope (SEM) micrographs of the Ti-3Sn-X alloys powder blends: a) Ti-3Sn-Nb, b) Ti-3Sn-Mo, and c) Ti-3Sn-Mn.

Table 1. Characteristics of the commercial raw powders as per suppliers' specification.

Powder	Max particle size [μm]	Morphology	Purity [%]	Supplier
Ti	<75	Irregular	>99.4	Goodfellow
Sn	<45	Spherical	>99.8	Sigma-Aldrich
Nb	<45	Irregular	>99.8	AlfAesar
Mo	<5	Rounded	>99.9	Sigma-Aldrich
Mn	<63	Angular	>99.0	Sigma-Aldrich

the samples were cold pressed into cylindrical specimens with 40 mm diameter and 10 mm thickness. Uniaxial pressing was done at room temperature by using a 100-Ton press applying 600 MPa of load and 15 s of holding time. As per current literature,[7,22,23] the specimens were subsequently vacuum sintered using 10 °C min^{-1} heating rate up to 1300 °C and held for 2 h. The specimens were finally cooled inside the furnace using a cooling rate of 10 °C min^{-1}.

For microstructural investigation, which was performed using an Olympus BX-60 optical microscope and a Hitachi S-4700 SEM, the samples were ground, polished, and etched with a water-based Kroll etchant (2 mL HF + 4 mL HNO_3). XRD analysis, which was performed on Philips X'pert equipment (radiation: CuK_α), was done using 0.013° as scanning rate in the 30°–80° 2θ scanning angle range.

The theoretical density of the alloys (g cm^{-3}) was calculated as the density of the individual element times the corresponding amount using the rule of mixtures. The dimensions (diameter and height) of the green samples were measured using a caliper while their weight was measured through a high-precision analytical scale. For the sintered materials, their density was obtained by measuring the weight of the material in air and water using Archimedes' principle of liquid displacement.

Dog-bone tensile testing samples with rectangular cross-sections $2 \times 2\ mm^2$ and a gauge length of 20 mm were obtained by means of a wire cutter. After cutting, the samples were ground to remove the surface roughness. For each composition, a minimum of three tensile specimens was tested using a constant crosshead speed of 0.1 mm min^{-1} in an Instron 33R4204 universal tensile tester equipped with a 50 kN load cell. Samples were mechanically fit in clamps with appropriate geometry and an external mechanical extensometer was used to continuously measure the elongation. Five individual measurements were performed to quantify the average Vickers microhardness (HV_1) of the alloys.

3. Results and Discussion

3.1. Design of the Ti-3Sn-X Alloys

In this study, we aimed at designing Ti-3Sn-X alloys (x = Nb, Mo, Mn) to investigate the effect of different β-stabilizing elements on their manufacturability and achievable properties. The design was done through a combination of the molybdenum equivalent parameter as defined by Wang et al.[24] and the molecular orbital method proposed by Morinaga.[25] It is worth mentioning that in the literature, there exist other definitions of the molybdenum equivalent parameter (e.g., Molchanova[26] or Bania[27]) but they do not take into account the effect of Sn. From **Figure 2**a), which shows the molybdenum equivalent parameter of the alloys of this study, it can be seen that the selected alloying elements have a proportionally higher β phase stabilization factor. Specifically, this factor increases from 0.28 for Nb, to 1 for Mo and to 2.26 for Mn. This allows to clarify the effect of β stabilizers with a factor lower (i.e., Nb) and higher (i.e., Mn) stabilization power, respectively, in comparison to Mo, which is commonly used as baseline. It can also be noticed that, as expected, the molybdenum equivalent parameter increases with the amount of each specific β stabilizer (Figure 2a). The subdivision proposed by Cotton et al.[28] was used and, therefore, the Ti-3Sn-Nb alloys are classified as near-β while the Ti-3Sn-Mo and Ti-3Sn-Mn alloys are metastable β.

Determination of the amount of each specific β stabilizer was refined by creating a bond order/*d*-orbital energy map (Figure 2b). One composition laying at the β alloys' borderline (thick dashed line) and one inside the β alloys' field were chosen. It is worth mentioning that the intrinsic diffusivity of the alloying elements, as dictated by their melting point, was also taken into account. Mn has higher diffusivity than Nb and Mo, which favors the dissolution of the powder particles.[6] Consequently, the relative position of the Ti-3Sn-Mn alloys in the bond order/*d*-orbital energy map is shifted toward inside the β alloys' field with respect to the Ti-3Sn-Nb and Ti-3Sn-Mo alloys. From this combined designing approach, the proposed alloys include Ti-3Sn-20Nb, Ti-3Sn-25Nb, Ti-3Sn-10Mo, Ti-3Sn-12Mo, Ti-3Sn-8Mn, and Ti-3Sn-10Mn (Figure 2).

3.2. Microstructural Analysis of the Ti-3Sn-X Alloys

Representative results of the microstructural characterization of the Ti-3Sn-Nb alloys are shown in **Figure 3** where it can be seen that the alloys are characterized by the presence of residual porosity. This is the expected behavior for powder metallurgy Ti-based alloys and the fact that the pores are isolated, almost spherical in shape, and primarily sitting at the grain boundaries (Figure 3a,b) indicates that the alloys reached the last stage of sintering during their manufacturing. Because of that, full dissolution of the alloying elements powder particles and achievement of a fully homogeneous chemistry is expected as it was confirmed via elemental mapping analysis. It can be noticed that the distribution of Ti (Figure 3f) and Sn (Figure 3g) is completely homogeneous between the phases composing the alloys whereas depletion of Nb (Figure 3h) is appreciable at the α grain boundaries. This is coherent with the equilibrium binary Ti-Nb phase diagram as the solubility of Nb in α Ti is approximately 3 wt%.[29] As near-β Ti alloys, the Ti-3Sn-Nb alloys have the classical lamellar microstructure constituted by equiaxed α grain boundaries and α + β lamellae. The size of the equiaxed α grains is not significantly different, although slightly smaller for the Ti-3Sn-25Nb alloy, and the lamellae are finer for higher amounts of Nb as a consequence of the greater amount of stabilized β phase (Figure 3c,d).

From the representative results of the microstructural characterization of the Ti-3Sn-Mo alloys, residual isolated rounded pores are present (**Figure 4**a,b), the alloys are characterized by a lamellar microstructure (Figure 4c,d), and homogenization of the alloying elements was obtained during sintering (Figure 4e–h) although of the high melting point of Mo. The complete dissolution of the Mo powder particles, despite the slow

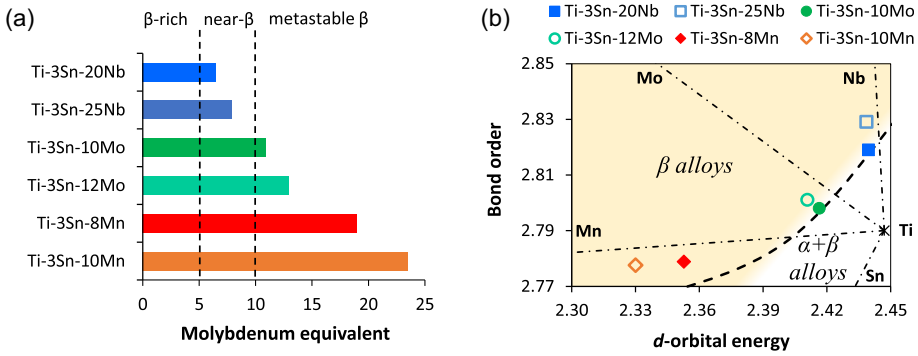

Figure 2. Details of the theories used to design the Ti-3Sn-X alloys (X = Nb, Mo, Mn): a) molybdenum equivalent, and b) bond order/*d*-orbital energy map.

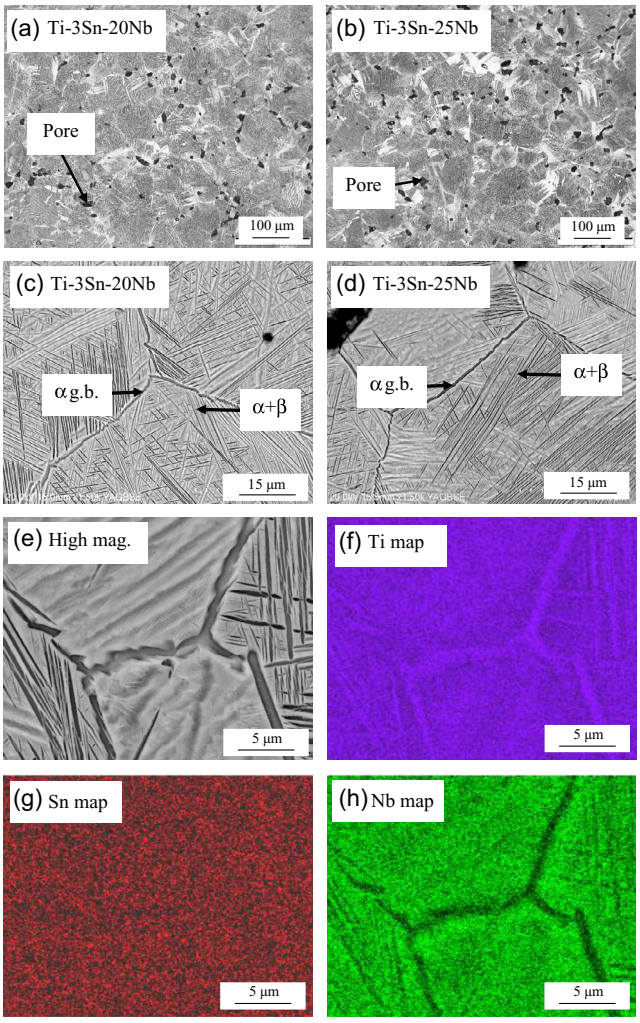

Figure 3. Representative results of the microstructural characterization of the Ti-3Sn-20Nb and Ti-3Sn-25Nb alloys, respectively: a,b) optical micrographs, c,d) SEM micrographs, e) high magnification SEM micrograph, f) Ti elemental map, g) Sn elemental map, and h) Nb elemental map.

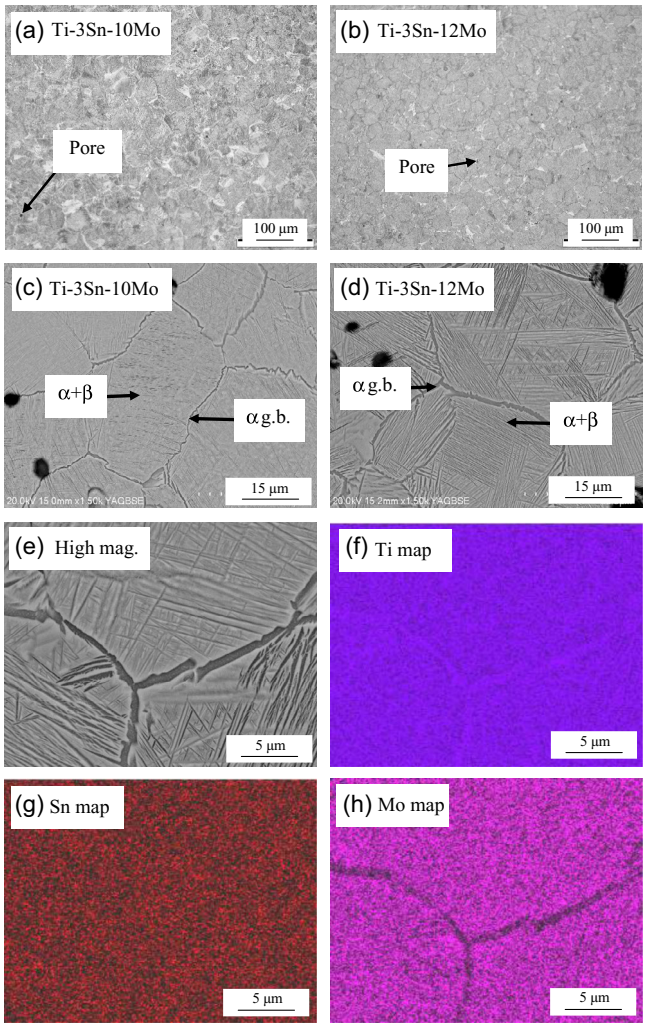

Figure 4. Representative results of the microstructural characterization of the Ti-3Sn-10Mo and Ti-3Sn-12Mo alloys, respectively: a,b) optical micrographs, c,d) SEM micrographs, e) high magnification SEM micrograph, f) Ti elemental map, g) Sn elemental map, and h) Mo elemental map.

diffusivity, is ascribable to their small particles size (Table 1). The only remarkable difference between the microstructure of the Ti-3Sn-Nb and Ti-3Sn-Mo alloys is the size of the features of the lamellar microstructure. In particular, the Ti-3Sn-Mo alloys are characterized by significantly smaller equiaxed α grains and finer lamellae, once again due to the higher amount of stabilized β phase. As for the Ti-3Sn-Nb alloys, despite the fact that both Nb and Mo are isomorphous β stabilizers, a noticeable depletion of Mo at the α grain boundaries is found (Figure 4h).

As for the other Ti-3Sn-X alloys, residual porosity is present in the microstructure of the sintered Ti-3Sn-Mn alloys where both spherical and irregular pores can be seen (**Figure 5**a,b). The chemical composition of the alloys is homogeneous due to the fast dissolution of the Sn and Mn powder particles. The key difference with respect to other Ti-3Sn-X alloys is that the Ti-3Sn-Mn alloys are characterized by a β-type microstructure composed of β grains and α lamellae found either at the grain boundaries or within the grains (Figure 5c,d) rather than the typical lamellar microstructure. The resulting microstructure is due to Mn having a stronger β-stabilizing effect compared to Nb and Mo. The amount of Mn added is high enough to form β grains but not sufficient to completely prevent the allotropic phase transformation. Consequently, α lamellae still form within the microstructure upon cooling from the sintering temperature. On average, the size of the grains is comparable to that of the Ti-3Sn-Nb alloys but the α lamellae are significantly coarser in the case of the Ti-3Sn-Mn alloys. Elemental mapping analysis shows a homogeneous distribution of Ti (Figure 5f) and Sn (Figure 5g) within the two phases but depletion of Mn in the α lamellae is clearly discernible (Figure 5h) as Mn has limited solubility in the α Ti phase.[29]

The results of the XRD characterization of the Ti-3Sn-X alloys are shown in **Figure 6**. From the XRD patterns of the Ti-3Sn-Nb alloys, it can be seen that the diffraction peak with the highest relative intensity is the one related to the β phase (Figure 6a). A substantial number of diffraction peaks corresponding to

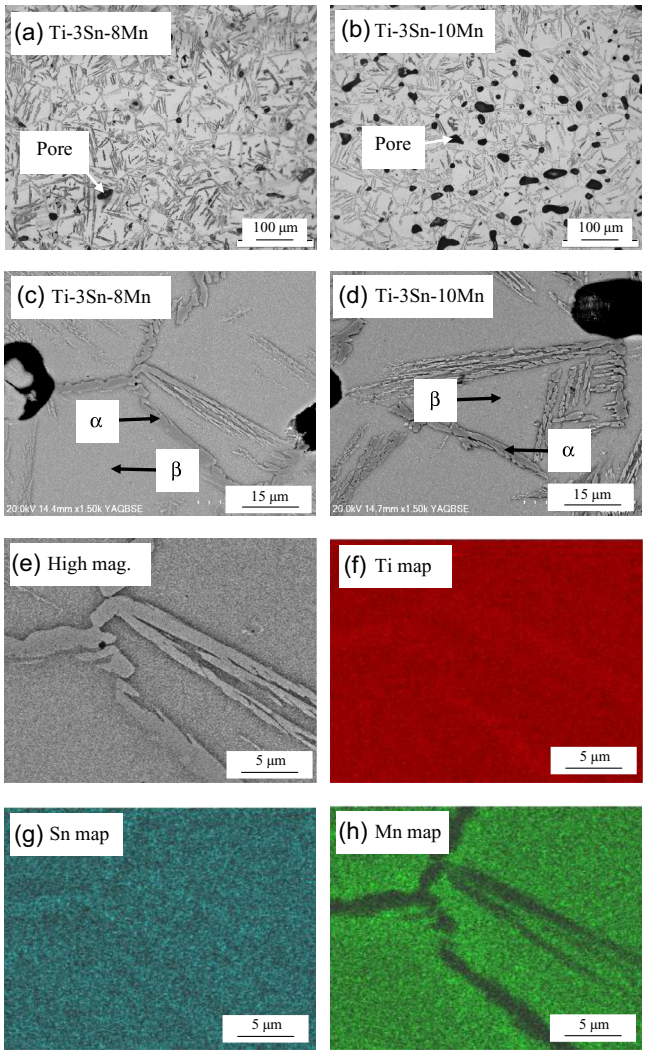

Figure 5. Representative results of the microstructural characterization of the Ti-3Sn-8Mn and Ti-3Sn-10Mn alloys, respectively: a,b) optical micrographs, c,d) SEM micrographs, e) high magnification SEM micrograph, f) Ti elemental map, g) Sn elemental map, and h) Mn elemental map.

the α phase are also present in agreement with the lamellar microstructure found during microstructural analysis (Figure 3). It can be noticed that as the amount of Nb increases the relative intensity of the α phase's peaks decreases, which is especially noticeable from the decrement of the relative intensity of the α(101) plane diffraction peak sitting at approximately 40°.

The analysis of the Ti-3Sn-Mo alloys yields similar results where the main diffraction peak of the β phase is the one with the highest relative intensity and the diffraction peaks of the α phase decrease in intensity when the amount of Mo is increased (Figure 6b). This is coherent with the stabilization of a greater amount of β phase within the microstructure (Figure 4) as brought about by using a higher content of β stabilizer. Key differences between the XRD patterns of the Ti-3Sn-Mn alloys (Figure 6c) with respect to the other Ti-3Sn-X alloys are the disappearance of the α(101) plane diffraction peak, which overlaps with the main peak of the β phase, and the detection of a third peak at around 72° related to the β phase. As expected, the relative intensity of the β phase's peaks increases with the amount of Mn added to the alloy due to the stabilization of a greater amount of β phase in the microstructure (Figure 5). The previously discussed behavior is consistent with the quantification of the variation of the amount of the two phases presented in Figure 6d) as the relative amount of α decreases and that of the β phase increases with the increment of the amount of each β stabilizer. Moreover, higher amounts of β phase are found when more powerful β stabilizers are used. Overall, the XRD analysis also confirms that the Ti-3Sn-X alloys are characterized by a homogeneous chemistry as no diffraction peaks related to the elemental powders were detected. Moreover, it is confirmed that no metastable and intermetallic phases are present in the sintered alloys, although they might have formed—especially when the melting of Sn occurs—and subsequently disappeared through the sintered process.

3.3. Physical Properties of the Ti-3Sn-X Alloys

Figure 7 shows the results of the characterization of the physical properties of the Ti-3Sn-X alloys. In terms of green density, regardless of the type of alloying element powder added, slightly higher values are obtained when using a greater amount of the same alloying elements, e.g., Nb. This means that the addition of an alloying element with a particle size lower than that of Ti (Table 1) slightly increases the compressibility of the Ti-3Sn-X alloy powder blends regardless of the actual morphology and size of the alloying element used. However, the latter, the actual amount of powder added as well as the intrinsic hardness do have an effect on the compressibility. Consequently, slightly higher green density values are progressively achieved by changing the main β stabilizer alloying element from Nb to Mo and, eventually, Mn.

Considering the relative density values of the sintered samples, it can be seen that for each system the alloys with higher amount of β stabilizer reach higher relative density values. As the samples were all sintered under the same conditions, this is due to the slightly higher green density. Nonetheless, the outcome of the sintering process is also significantly affected by the particle size of the alloying elements and their intrinsic diffusivity at the sintering temperature. Specifically, among the β stabilizer alloying elements used, Mn has the lowest melting point followed by Nb and then Mo. Therefore, for the same sintering temperature, the intrinsic diffusivity progressively decreases from Mn to Nb and Mo. However, the particle size of the powders used decreases from Mn to Nb and Mo, with Mo having a significantly smaller size than the other β stabilizer alloying element (Table 1). The combination of these factors justifies the trend obtained where, in general, the Ti-3Sn-Nb and Ti-3Sn-Mo alloys have slightly higher sintered density values compared to the Ti-3Sn-Mn alloys despite starting from a lower green density (Figure 7a). Such behavior is reflected in the densification parameter values plotted in Figure 7b) where, overall, higher densification is achieved through the addition of Mo followed by Nb and Mn. Additionally, the densification value increases with the amount of β stabilizer alloying element for each Ti-3Sn-X alloy system. Accordingly, it can be seen that the porosity gap within

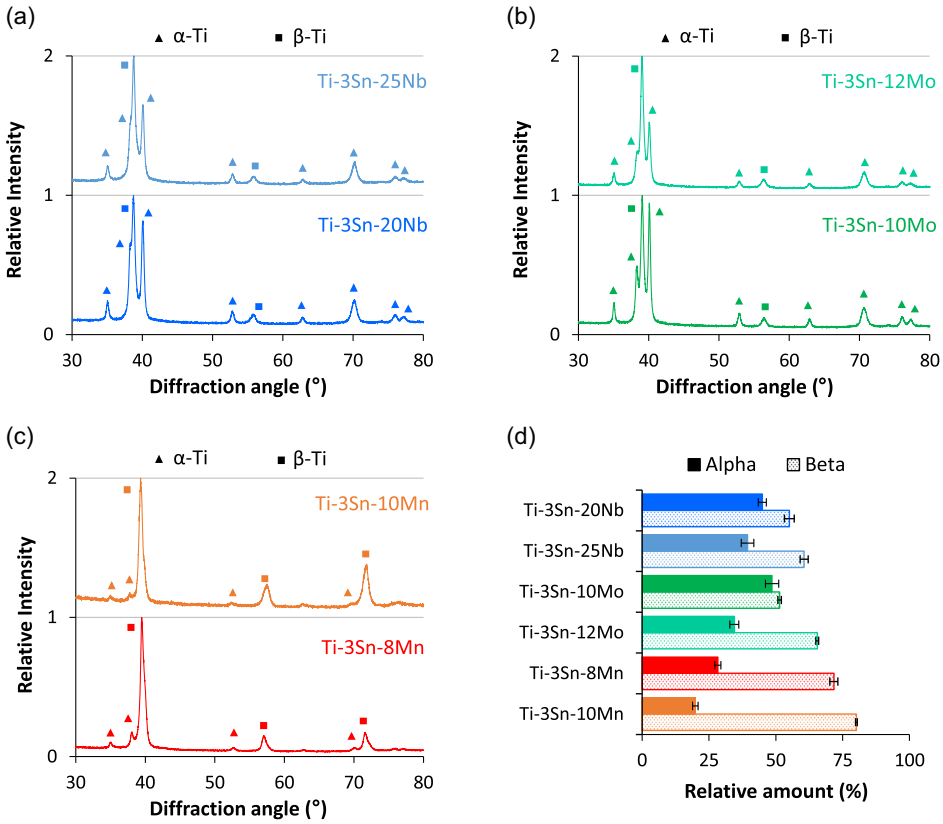

Figure 6. Results of the XRD analysis of the Ti-3Sn-X alloys: a) XRD patterns of the Ti-3Sn-Nb alloys, b) XRD patterns of the Ti-3Sn-Mo alloys, c) XRD patterns of the Ti-3Sn-Mn alloys, and d) relative amount of the α and β phases.

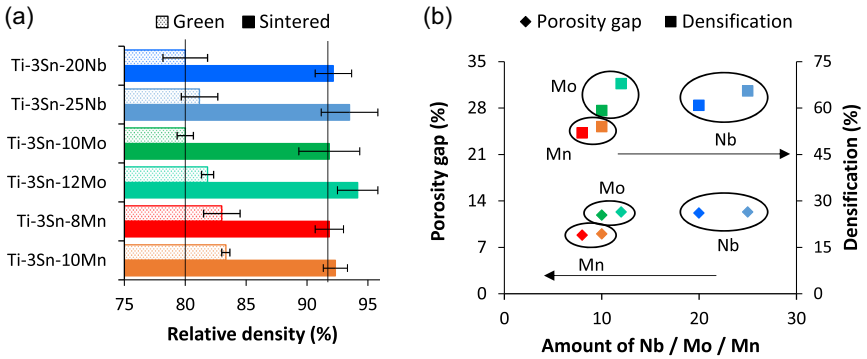

Figure 7. Results of the characterization of the physical properties of the Ti-3Sn-X alloys (X = Nb, Mo, Mn): a) relative density, and b) porosity gap and densification as a function of the amount of β stabilizer.

each system is marginally higher for greater addition rates of β stabilizer alloying elements and the Ti-3Sn-Nb and Ti-3Sn-Mo alloys have higher porosity gap values with respect to the Ti-3Sn-Mn alloys. It is worth noticing that the relative density data presented in Figure 7a) are coherent with the volumetric amount of residual porosity present in the microstructures of the Ti-3Sn-X alloys (Figure 3–5). It is also worth mentioning that, independently of the small differences found, the green and sintered relative density values of the Ti-3Sn-X alloys (Figure 7) are comparable to those of other Ti alloys manufactured via the blended elemental powder metallurgy method.[7,30,31]

3.4. Mechanical Behavior of the Ti-3Sn-X Alloys

Representative stress–strain tensile curves as well as the average mechanical properties of the Ti-3Sn-X alloys are reported in **Figure 8**. It is found that the Ti-3Sn-Nb and Ti-3Sn-Mo alloys are characterized by both elastic and plastic deformation before noncatastrophic failure while the Ti-3Sn-Mn alloys show pure elastic behavior. For each system, the stiffness is not greatly affected by the amount of alloying elements, but the Young modulus significantly changes depending on the type of β stabilizer alloying element considered. Ti-3Sn-Mo alloys are stiffer compared to

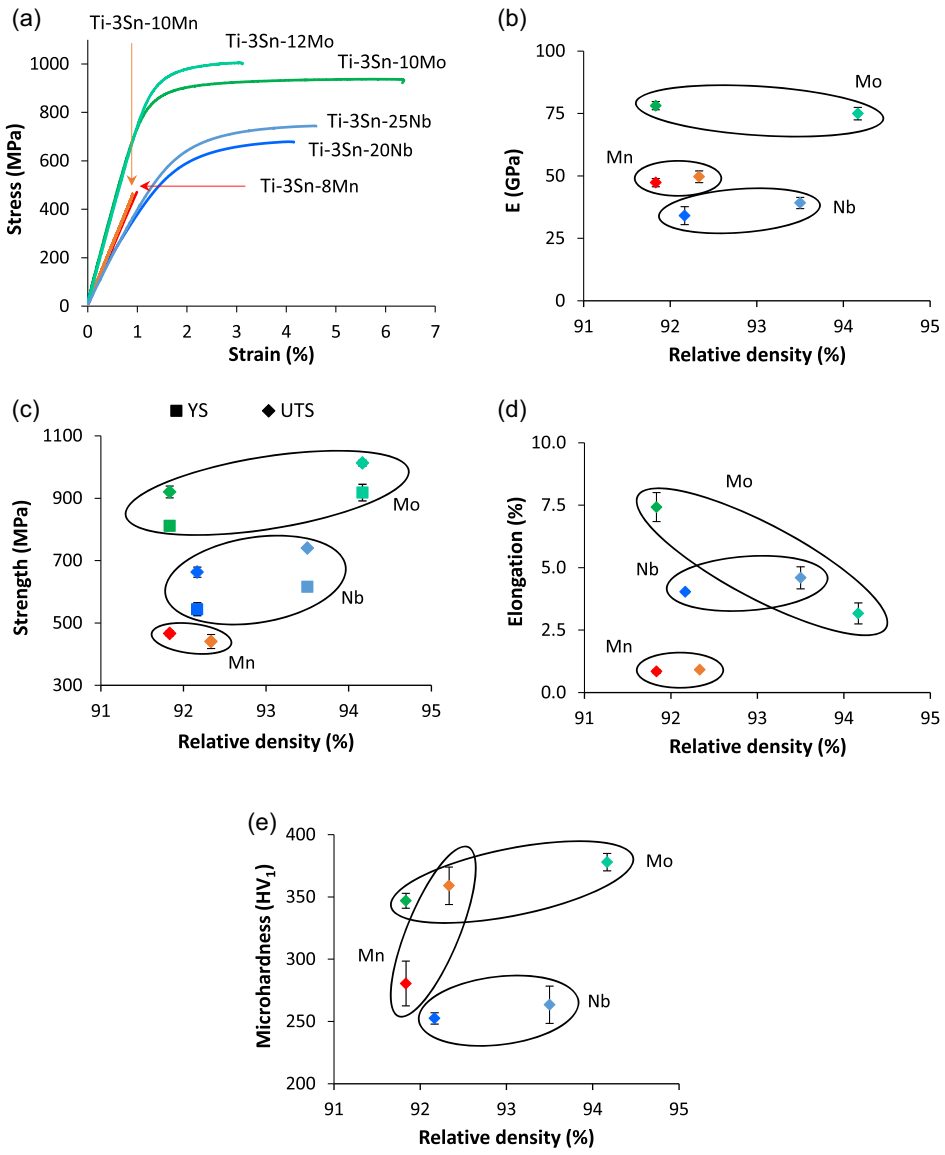

Figure 8. Results of the characterization of the mechanical behavior of the Ti-3Sn-X alloys (X = Nb, Mo, Mn): a) representative stress/strain curves, b) Young modulus versus sintered density), c) strength versus sintered density, d) elongation versus sintered density, and e) hardness versus sintered density.

the Ti-3Sn-Mn and Ti-3Sn-Nb alloys (Figure 8b). Similar Young modulus' values were reported in the literature for Ti-Mo alloys,[32] Ti-Nb-Zr alloys.[33] and Ti-Nb-Sn alloys,[34,35] respectively.

With respect to the strength of the Ti-3Sn-X alloys (Figure 8c), generally the increase of the amount of the β stabilizer alloying element increases the strength with the exception of the Ti-3Sn-Mn alloys where the ultimate tensile strength (UTS) slightly decreases due to the brittle nature of the alloys. More in detail, the increase of the Nb content from 20% to 25% leads to an average increase of the YS and UTS of 75 MPa while an average increase of 100 MPa is achieved when increasing the Mo content from 10% to 12%. The higher strengthening induced by the addition of Mo is due to its stronger β-stabilizing effect. Consequently, the Ti-3Sn-Mo alloys are stronger (250–300 MPa) than the Ti-3Sn-Nb alloys despite their lower total amount of alloying elements. Even higher strength values should have been achieved in the Ti-3Sn-Mn alloys; however, that is prevented by their premature catastrophic failure.

The variation in the strength of the Ti-3Sn-X alloys is justified by the compromise between the different aspects brought about by the addition of each specific alloying element including solid solution, microstructural changes, and residual porosity. In particular, the contribution of the solid solution strengthening mechanism is proportional to the amount of alloying elements added. The associated maximum solubility of the elements in the phases present in the microstructure is also relevant as this leads to partitioning as shown by the microstructural analysis. Regardless of the type of β stabilizer considered, their addition leads to the stabilization of a greater amount of the β phase which is stronger than the α phase. Additionally, the addition of the β

stabilizers generates microstructures composed of slightly smaller equiaxed α grains and significantly finer α + β lamellae with attendant reduction of the interlamellar spacing. It is found that the contribution of the strengthening via microstructural refinement becomes more prominent moving from Nb to Mo and to Mn. In this instance, the addition of a higher amount of each β stabilizer also leads to a lower amount of residual porosity which constitutes stress concentration sites and can provide a preferential pathway for crack propagation. All these aspects are therefore responsible for the continuous increase of the resistance to plastic deformation, resulting in the increase of the strength, as shown in Figure 8c).

Regarding the elongation at failure (Figure 8d), it is expected that lower ductility values are achieved for stronger alloys. It can be noticed that this is only the case for the Ti-3Sn-Mo alloys whereas the ductility increases with the amount of Nb and remains constant with the amount of Mn. For the latter, the elongation at failure Ti-3Sn-Mn alloys does not significantly change because of the purely elastic behavior. For the Ti-3Sn-Nb alloys, the elongation at failure slightly increases due to the better compromise between increase in relative density (Figure 7), higher amount of stabilized α phase (Figure 6), and less pronounced refinement of the lamellar structure (Figure 3) in comparison to the Ti-3Sn-Mo alloys (Figure 4). As for the strength, the variation of the elongation at failure is related to the effects caused by the addition of the β stabilizers and their actual amount. On the one side, all the strengthening mechanisms previously mentioned, which include solid solution, stabilization of the β phase, and refinement of the microstructural features are detrimental for the ductility. On the other side, the reduction of the total amount of residual pores present in the microstructure is beneficial. Therefore, for each specific alloying elements, their compromise justifies the trends shown in Figure 8d).

Due to the well-established relationship between strength and hardness, similar trends are obtained in terms of Vickers microhardness (Figure 8e). Therefore, the hardness increases with the amount of the β stabilizer alloying element for each system. Moreover, the increment of the Mn content leads to a greater increase in hardness (79 HV_1) compared to the incremental addition of Mo (31 HV_1) and Nb (11 HV_1). This is obviously related to the β stabilizing power of each alloying element and the resultant microstructure. Accordingly, the Ti-3Sn-Mo alloys are characterized by higher hardness values (95–115 HV_1) with respect to the Ti-3Sn-Nb alloys. The hardness of the Ti-3Sn-10Mn alloy is comparable to that of the Ti-3Sn-Mo alloys and the hardness of the Ti-3Sn-8Mn alloy is more similar to that of the Ti-3Sn-Nb alloys. Consequently, all the aspects previously mentioned (i.e., solid solution strengthening, increased amount of β phase, finer lamellar structure, and the decrement of the volumetric amount of residual porosity) contribute to make the Ti-3Sn-X alloys harder for higher additions of β stabilizers as a function of their β stabilization power (Nb→Mo→Mn).

From Figure 8, it can also be appreciated the effect of the relative sintered density. Generally higher performance is achieved when reaching higher relative density, which is the expected behavior for powder metallurgy materials.[36] The higher increment in density in the Ti-3Sn-Mo alloys contributes to justify their higher mechanical properties with respect to the Ti-3Sn-Nb alloys. The rate at which the strength and hardness of these alloys increase with the relative density for each alloy system is fairly similar. This is due to the compromise between the different strengthening effects brought about by the addition of Mo and Nb, which include solid solution strengthening, microstructural refinement (Figure 3–5), stabilization of a greater amount of β phase (Figure 6), and changes in amount of residual porosity (Figure 2). However, it is interesting to notice the remarkably higher increase in hardness over a small relative density range of the Ti-3Sn-Mn alloys (Figure 8e). Such an increment is due to the much stronger β-stabilizing effect of Mn and the consequent formation of a β-type microstructure (Figure 5) rather than a lamellar one. It is worth noting that the mechanical properties discussed are also affected by the amount of interstitials in general and oxygen in particular as they are renowned to strengthen Ti alloys. The Ti-3Sn-X alloys have an oxygen content greater than 0.2 wt%, which is commonly specified for wrought alloys, as a consequence of the oxygen content of the raw Ti powder used.

Representative results of the fractographic analysis of the Ti-3Sn-X alloys are shown in **Figure 9**. From their comparison, it is evident the difference in fracture mode between the Ti-3Sn-Nb and Ti-3Sn-Mo alloys and the Ti-3Sn-Mn alloys. Due to their purely elastic behavior, the Ti-3Sn-Mn alloys fail in a brittle manner and, therefore, the fracture surface is flat, cleavage planes are clearly discernible, river pattern left by transgranular interlamellar failure are present, and the morphology of the residual pores is mainly undeformed. Conversely, the fracture surface of the

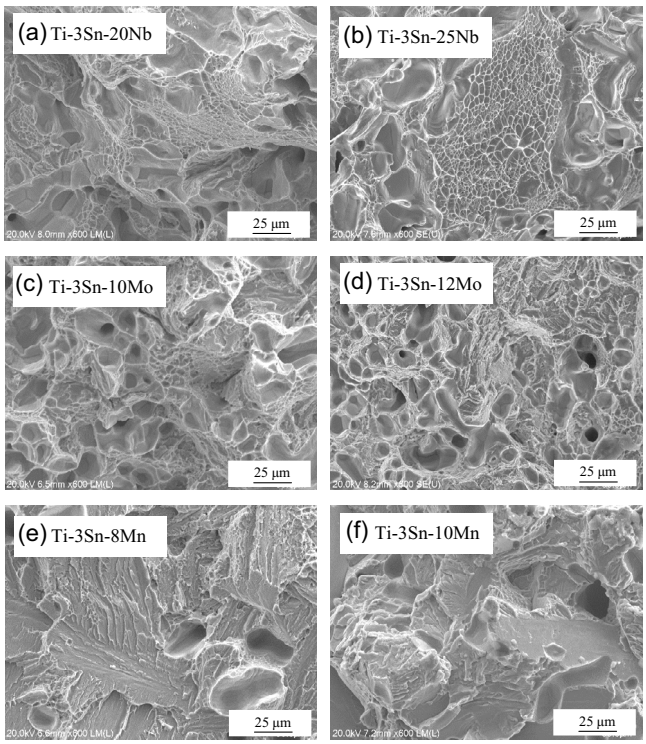

Figure 9. Representative results of the fractographic analysis characterization of the Ti-3Sn-X alloys: a) Ti-3Sn-20Nb alloy, b) Ti-3Sn-25Nb alloy, c) Ti-3Sn-10Mo alloy, d) Ti-3Sn-12Mo alloy, e) Ti-3Sn-8Mn alloy, and f) Ti-3Sn-10Mn alloy.

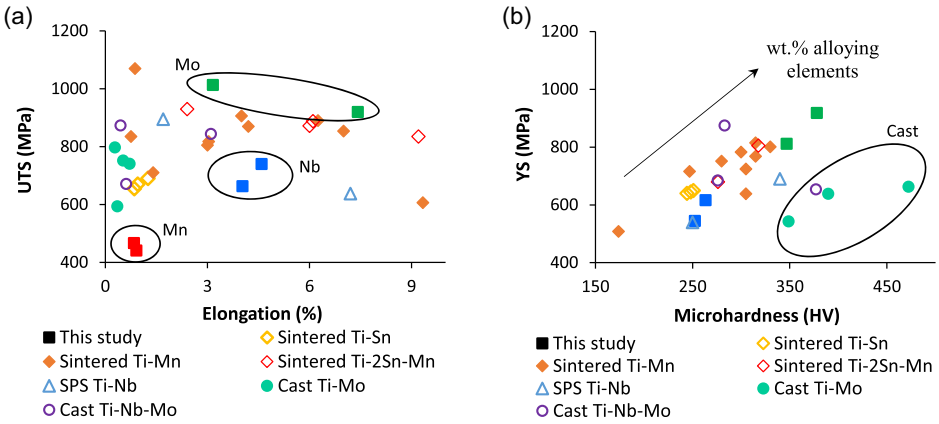

Figure 10. Comparison of the mechanical properties of the Ti-3Sn-X alloys (X = Nb, Mo, Mn) with other Ti alloys bearing Sn, Nb, Mo, and Mn as alloying elements:[13,18,21,37–41] a) UTS versus elongation and b) YS versus hardness.

Ti-3Sn-Nb and Ti-3Sn-Mo alloys is rough as a consequence of their ductile behavior. Specifically, dimples and deformed residual pores are the primary constituents of the fracture surface, even though some shallow t-ridges derived by the intergranular fracture of the colonies' boundaries are also found. The results of the fractographic analysis are consistent with the tensile behavior (Figure 8) and, thus, a greater number of ductile dimples are generally found in the Ti-3Sn-Nb alloys. However, the fracture surface of the Ti-3Sn-8Mo alloy has a significant amount of areas failed in a ductile manner due to the ability of this alloy to withstand a great amount of plastic deformation before failure.

Figure 10 shows the comparison of the mechanical properties (UTS/elongation and YS/hardness) of the Ti-3Sn-X alloys with other Ti alloys bearing the alloying elements of the Ti-3Sn-X alloys produced by different manufacturing methods. In term of strength/ductility pairs, the Ti-3Sn-Mo alloys show the best compromise with higher strength for comparable ductility with respect to sintered Ti-Mn and Ti-2Sn-Mn alloys, remarkably higher strength and ductility in comparison to sintered Ti-Sn alloys as well as higher strength and significantly better elongation compared to cast Ti-Mo and Ti-Nb-Mo alloys. The Ti-3Sn-Nb alloys have similar UTS but higher elongation compared to sintered Ti-Sn alloys, the strength is comparable or lower but the ductility is higher in comparison to cast Ti-Nb-Mo alloys, and the UTS/elongation pairs seem to be comparable to those of spark plasma sintered Ti-Nb alloys. Due to their brittle nature, the Ti-Nb-Mn alloys have the lowest UTS/elongation pairs, although their ductility is still comparable to that of sintered Ti-Sn alloys and cast Ti-Mo alloys. The highlighted differences derive from the type of manufacturing route used as well as the actual composition of each specific alloy. In particular, binary Ti-(2.5–7.5)Sn,[13] Ti-(15–25)Nb,[37] Ti-(8.7–15)Mo,[38] Ti-(1–14)Mn,[18,39,40] ternary Ti-(10.8–26.7)Nb-(9.2–10.8)Mo,[41] and Ti-(2)Sn-(2–4)Mn[21] alloys were used for the sake of comparison. In general, the higher the amount of alloying elements the higher the strength and the lower the ductility, and alloys obtained via powder metallurgy show better ductility than those manufactured via casting. This is derived by the fact that a greater amount of alloying elements generally leads to the activation of different strengthening mechanisms among which a proportionally higher solid solution strengthening, greater amount of β phase stabilized within the lamellar microstructure, and refinement of the microstructural features. The use of powder metallurgy to fabricate the Ti alloys generally results in finer microstructure with respect to casting but powder metallurgy materials are also characterized by presence of residual porosity.

Analyzing the variation of YS versus hardness (Figure 10b), a greater amount of alloying elements in the composition lead to stronger and harder materials regardless of the type of alloying element used. Moreover, cast alloys have normally higher hardness for comparable YS values. On the one side, the Ti-3Sn-Mo alloys are characterized by the highest YS/hardness pairs with respect to all the other powder metallurgy alloys considered, including sintered Ti-Sn, sintered Ti-Mn, and sintered Ti-2Sn-Mn alloys. On the other side, the Ti-3Sn-Nb alloys are characterized by the lowest YS/hardness pairs among the powder metallurgy alloys. Moreover, the Ti-3Sn-Nb alloys have comparable YS and lower hardness with respect to some of cast of the Ti-Mo alloys. However, it is worth mentioning that the comparison of the YS/hardness pairs is also affected by the fact that slightly different types of Vickers microhardness (i.e., $HV_{0.2}$, $HV_{0.3}$, $HV_{0.5}$, and HV_1) were used in the different studies.

4. Conclusion

This study analyzed the design and manufacturing via powder metallurgy of ternary Ti-3Sn-X alloys (X = Nb, Mo, Mn) and aims to gain an understanding of the effects that the different β stabilizers have on the microstructure and properties. It can be concluded that ternary Ti-3Sn-X alloys with homogeneous chemistry can be achieved regardless of their actual composition when using the commercial powders described in this study. The complete dissolution of the alloying elements powder particles is favored by either their high diffusivity in Ti at the chosen sintering temperature or their small particle size. The designed Ti-3Sn-Nb and Ti-3Sn-Mo alloys are characterized by a lamellar microstructure that is refined if higher additions of alloying elements are used. Moreover, the Ti-3Sn-Mo alloys have finer microstructural features in comparison to Ti-3Sn-Nb alloys

due to the stronger β stabilizing power of Mo. For the same reason, the designed Ti-3Sn-Mn alloys are characterized by a β-type microstructure. The selection of the alloying elements powder is crucial as their particle size and morphology affect the compressibility and the sinterability of the ternary Ti-3Sn-X alloys, which in this instance are both enhanced. Due to the resulting microstructure and associated strengthening mechanisms, the Ti-3Sn-Nb and Ti-3Sn-Mo alloys show elastoplastic behavior while the Ti-3Sn-Mn alloys are brittle in nature and this is reflected in their fracture surface. Strength, hardness, and ductility are improved by higher additions of Nb whereas Mo enhances the strength but decreases the ability to plastically deform. The Ti-3Sn-Mo alloys have the best compromise between strength and ductility among the alloys studied and those available in literature used for the sake of comparison.

Acknowledgements

This research did not receive any specific grant from funding agencies in the public, commercial, or not-for-profit sectors. The authors acknowledge the technical contribution of Miss Maryam Al-Hajri.

Open access publishing facilitated by The University of Waikato, as part of the Wiley - The University of Waikato agreement via the Council of Australian University Librarians.

Conflict of Interest

The authors declare no conflict of interest.

Data Availability Statement

The data that support the findings of this study are available from the corresponding author upon reasonable request.

Keywords

blended elemental, homogeneous microstructures, mechanical properties, powder metallurgy, titanium alloys

Received: September 17, 2023
Revised: November 7, 2023
Published online:

[1] M. A. Imam, F. H. S. Froes, R. G. Reddy, *Key Eng. Mater.* **2013**, *551*, 3.
[2] L. Bolzoni, M. Xia, N. Hari Babu, *Sci. Rep.* **2016**, *6*, 39554.
[3] R. M. German, *Int. J. Refract. Met. Hard Mater.* **2020**, *89*, 105214.
[4] C. G. McCracken, C. Motchenbacher, D. P. Barbis, *Int. J. Powder Metall.* **2010**, *46*, 19.
[5] L. Bolzoni, E. M. Ruiz-Navas, E. Gordo, *Mater. Chem. Phys.* **2012**, *137*, 608.
[6] A. Amherd Hidalgo, R. Frykholm, T. Ebel, F. Pyczak, *Adv. Eng. Mater.* **2017**, *19*, 1600743.
[7] H. Wang, Z. Z. Fang, P. Sun, *Int. J. Powder Metall.* **2010**, *46*, 45.
[8] S. Raynova, M. A. Imam, F. Yang, L. Bolzoni, *J. Manuf. Process.* **2019**, *39*, 52.
[9] A. Amigó-Mata, M. Haro-Rodriguez, Á. Vicente-Escuder, V. Amigó-Borrás, *Powder Metall.* **2022**, *65*, 31.
[10] B.-Y. Chen, K.-S. Hwang, *Mater. Sci. Eng. A* **2012**, *541*, 88.
[11] L. Bolzoni, E. M. Ruiz-Navas, E. Gordo, *Mater. Sci. Eng. A* **2014**, *609*, 266.
[12] Q. Cai, C. Xu, X. Chen, W. Xi, J. Cheng, Z. Chen, J. Chen, *J. Alloys Compd.* **2023**, *947*, 169608.
[13] H.-W. Liu, D. Paul Bishop, K. P. Plucknett, *Mater. Sci. Eng. A* **2015**, *644*, 392.
[14] A. Azmat, M. Tufail, A. D. Chandio, *Materials* **2021**, *14*, 7660.
[15] X. X. Ye, B. Chen, J. H. Shen, J. Umeda, K. Kondoh, *J. Alloys Compd.* **2017**, *709*, 381.
[16] D. Zhao, K. Chang, T. Ebel, M. Qian, R. Willumeit, M. Yan, F. Pyczak, *J. Mech. Behav. Biomed. Mater.* **2013**, *28*, 171.
[17] P. Sochacka, A. Miklaszewski, M. Jurczyk, *J. Alloys Compd.* **2019**, *776*, 370.
[18] P. Fernandes Santos, M. Niinomi, H. Liu, K. Cho, M. Nakai, Y. Itoh, T. Narushima, M. Ikeda, *J. Mech. Behav. Biomed. Mater.* **2016**, *59*, 497.
[19] E. Yılmaz, A. Gökçe, F. Findik, H. Özkan Gülsoy, *Vacuum* **2017**, *142*, 164.
[20] T. Maeshima, M. Nishida, *Mater. Trans.* **2004**, *45*, 1096.
[21] X. Zhou, H. Fang, T. Yuan, R. Li, *Mater. Charact.* **2023**, *203*, 113068.
[22] L. Bolzoni, M. Paul, F. Yang, *J. Mater. Res. Technol.* **2022**, *21*, 3828.
[23] T. Sjafrizal, A. Dehghan-Manshadi, D. Kent, M. Yan, M. S. Dargusch, *J. Mech. Behav. Biomed. Mater.* **2020**, *102*, 103518.
[24] Q. Wang, C. Dong, P. K. Liaw, *Metall. Mater. Trans. A* **2015**, *46*, 3440.
[25] M. Morinaga, *Mater. Trans.* **2016**, *57*, 213.
[26] K. Molchanova, *Phase Diagrams of Titanium Alloys, Translation of Atlas Diagram Sostoyaniya Titanovyk Splavov)*, Israel Program for Scientific Translations, Jerusalem **1965**, p. 154.
[27] P. J. Bania, *JOM* **1994**, *46*, 16.
[28] J. D. Cotton, R. D. Briggs, R. R. Boyer, S. Tamirisakandala, P. Russo, N. Shchetnikov, J. C. Fanning, *JOM* **2015**, *67*, 1281.
[29] J. L. Murray, *Phase Diagrams of Binary Titanium Alloys*, 1st ed., ASM International **1987**.
[30] M. T. Jia, B. Gabbitas, L. Bolzoni, *J. Mater. Process. Technol.* **2018**, *255*, 611.
[31] P. Kumar, K. S. R. Chandran, *Metall. Mater. Trans. A* **2017**, *48*, 2301.
[32] W.-D. Zhang, Y. Liu, H. Wu, M. Song, T.-Y. Zhang, X.-D. Lan, T.-H. Yao, *Mater. Charact.* **2015**, *106*, 302.
[33] Q. Liu, Q. Meng, S. Guo, X. Zhao, *Prog. Nat. Sci.: Mater. Int.* **2013**, *23*, 562.
[34] S. Hanada, N. Masahashi, S. Semboshi, T. K. Jung, *Mater. Sci. Eng. A* **2021**, *802*, 140645.
[35] S. Cai, L. Wang, J. E. Schaffer, J. Gao, Y. Ren, *Mater. Sci. Eng. A* **2019**, *743*, 764.
[36] L. Bolzoni, M. Alqattan, L. Peters, Y. Alshammari, F. Yang, *Sci. Rep.* **2020**, *10*, 22201.
[37] N. Suesawadwanid, A. Khantachawana, K. Srirussamee, K. Kondoh, *Powder Metall.* **2022**, *65*, 426.
[38] N. Moshokoa, L. Raganya, B. A. Obadele, R. Machaka, M. E. Makhatha, *Int. J. Adv. Manuf. Technol.* **2020**, *111*, 1237.
[39] Y. Alshammari, F. Yang, L. Bolzoni, *J. Mech. Behav. Biomed. Mater.* **2019**, *91*, 391.
[40] K. Cho, M. Niinomi, M. Nakai, J. Hieda, P. Fernandes Santos, Y. Itoh, M. Ikeda, *Biomaterials Science: Processing, Properties and Applications IV*, Vol. *251*, Wiley, NY, USA **2014**, pp. 21–30.
[41] L. Raganya, N. Moshokoa, B. Obadele, E. Makhatha, R. Machaka, *Int. J. Adv. Manuf. Technol.* **2021**, *115*, 3053.